Journal of Computational Physics **162,** 385–394 (2000)
doi:10.1006/jcph.2000.6543, available online at http://www.idealibrary.com on IDEAL®

# Modelling Phase Change with Dissipative Particle Dynamics Using a Consistent Boundary Condition

S. M. Willemsen, H. C. J. Hoefsloot, D. C. Visser, P. J. Hamersma, and P. D. Iedema

*Department of Chemical Engineering, University of Amsterdam, Nieuwe Achtergracht 166, 1018 WV Amsterdam, The Netherlands*
E-mail: sanderw@its.chem.uva.nl, huubh@its.chem.uva.nl, visser@its.chem.uva.nl, hamersma@its.chem.uva.nl, piet@its.chem.uva.nl

Received November 8, 1999; revised February 28, 2000

With the introduction of an energy-conserving dissipative particle dynamics (DPD) scheme, simulations of the thermal behaviour of complex fluids at hydrodynamic time scales became possible. In this paper it is demonstrated that a different equation of state allows us to perform simulations of the phase change of materials. We indicate that thermal simulations with a constant temperature boundary condition are only possible in an accurate way at high overlapping coefficients, if a newly developed consistent boundary condition is used. 

*Key Words:* dissipative particle dynamics; phase change; boundary condition.

## 1. INTRODUCTION

Dissipative particle dynamics has been introduced [1] as a method to simulate complex fluids. The idea is to simulate the motions of a collective of molecules (called fluid particles) rather than separate ones, which is common in molecular dynamics. The interaction between the particles is not only through a conservative force but also by a drag and a random force, springing from Brownian dynamics. With this choice of forces, this simulation method acts in the mesoscopic regime, and the hydrodynamic behaviour of complex fluids can be modelled. It can solve a variety of systems, ranging from suspensions [2] to dilute polymer solutions [3]. Also, phase separation has been studied using standard DPD [4], or a combination of DPD and advanced Monte Carlo techniques [5]. Besides these applications, theoretical progress has been made also. Español and Warren [6] derived the proper relationship between the interacting forces. Subsequently Español [7] and Marsh *et al.* [8] proved the true hydrodynamic behaviour of DPD.

The original method [1] could only simulate isothermal systems and consequently was not able to simulate heat transfer problems. Avalos and Mackie [9] and Español [10] solved



0021-9991/00 $35.00

this simultaneously by introducing an internal energy variable and a temperature for every particle. In this paper we have extended this model to allow for a phase change within the DPD simulation. In the next sections the model will be introduced together with a new, consistent boundary condition. Finally, the results of the phase change DPD scheme are presented.

## 2. THEORY

In this section the theory of energy-conserving dissipative particle dynamics will be explained. Subsequently, the necessary conditions to simulate a phase change will be presented.

### 2.1. *Energy-Conserving DPD*

Dissipative particle dynamics is a simulation technique for simulating complex fluids at hydrodynamic time scales. The DPD scheme consists of the calculation of the position and momenta of interacting (fluid) particles over time. The energy-conserving form also introduces an internal energy and a temperature for every particle.

The equations of motion for these particles with positions $\mathbf{r}_i(t)$ and momenta $\mathbf{p}_i(t)$ are given by

$$\begin{aligned} d\mathbf{r}_i &= \mathbf{v}_i\, dt \\ d\mathbf{v}_i &= \sum_{j\neq i}\left[a_{ij}\left(1-\frac{r_{ij}}{r_c}\right)\hat{\mathbf{r}}_{ij} - \gamma_{ij}\omega_D(r_{ij})(\hat{\mathbf{r}}_{ij}\cdot\mathbf{v}_{ij})\hat{\mathbf{r}}_{ij}\right]dt + \sigma_{ij}\omega_R(r_{ij})\theta_{ij}^V\hat{\mathbf{r}}_{ij}, \end{aligned} \tag{1}$$

where $a_{ij}$ is the maximum repulsion between particles $i$ and $j$, $\mathbf{r}_{ij}=\mathbf{r}_i-\mathbf{r}_j$, $r_{ij}=|\mathbf{r}_{ij}|$, $\hat{\mathbf{r}}_{ij}=\mathbf{r}_{ij}/|\mathbf{r}_{ij}|$, and $r_c$ is the cutoff radius. The second and third parts result from the dissipative and random interactions, with $\mathbf{v}_{ij}=\mathbf{v}_i-\mathbf{v}_j$, $\omega(r_{ij})$ as a weight function, which tends to zero for $r\to r_c$, and $\theta_{ij}^V$ is a random number with zero mean and $dt$ variance.

In the original DPD algorithm the friction coefficient $\gamma_{ij}$ and the noise amplitude $\sigma_{ij}$ were assumed to be identical for all particles, and these parameters were related to the temperature through a fluctuation–dissipation theorem $\sigma^2=2k_BT\gamma$ [6]. Since in energy-conserving DPD every particle may have a different temperature, Español [10] suggests keeping the noise amplitude constant for all particles and determining the friction constant from the fluctuating temperatures,

$$\gamma_{ij}=\frac{\sigma^2}{4}\left[\frac{1}{T_i}+\frac{1}{T_j}\right], \tag{2}$$

where $T_i$ is the temperature of particle $i$. Then the evolution of the internal energy $\epsilon_i$ is given by

$$\begin{aligned} d\epsilon_i = {} & \frac{1}{2}\left[\sum_j\left[\omega_D(r_{ij})\gamma_{ij}(\mathbf{v}_{ij}\cdot\hat{r}_{ij})^2-\sigma_{ij}^2\omega_R^2(r_{ij})\right]dt-\sum_j\sigma_{ij}\omega_R(r_{ij})(\mathbf{v}_{ij}\cdot\hat{r}_{ij})\theta_{ij}^V\right] \\ & +\sum_j\kappa_{ij}\left(\frac{1}{T_i}-\frac{1}{T_j}\right)\omega_{TD}(r_{ij})\,dt+\sum_j\alpha_{ij}\omega_{TR}(r_{ij})\theta_{ij}^T. \end{aligned} \tag{3}$$

The upper part of this equation is related to viscous heating of the particles, while the lower part is related to the conduction of heat. Here, $\kappa_{ij}$ represents a thermal conductivity that depends on the internal energy of particles $i$ and $j$ and follows from [10]

$$\kappa_{ij} = \frac{\tilde{\kappa}}{\lambda^2} \frac{T_i + T_j}{2} \frac{\epsilon_i + \epsilon_j}{2}. \tag{4}$$

Here, $\lambda$ is the average distance between particles and $\tilde{\kappa}$ is the thermal conductivity.

Finally, the detailed balance condition requires that $\alpha_{ij} = 2\kappa_{ij}^2$ and the relationship between the weight functions [6]

$$\begin{aligned} \omega_{\mathrm{R}}^2(r_{ij}) &= \omega_{\mathrm{D}}(r_{ij}) \\ \omega_{\mathrm{TR}}^2(r_{ij}) &= \omega_{\mathrm{TD}}(r_{ij}) \end{aligned} \tag{5}$$

with $k_{\mathrm{B}}$ the Boltzmann constant.

### 2.2. *Phase-Change DPD*

In the previous section the energy-conserving DPD model was described, which until now has been used for one-phase calculations only. In this case it may be assumed that the material has a constant heat capacity, independent of the internal energy. Español [10] suggests the equation of state

$$T(\epsilon) = \frac{\epsilon}{C_v} \tag{6}$$

with $C_v$ as the heat capacity of the substance to be simulated.

In the case of a material that changes phase, three stages can be defined. First, the material is solid (with a solid heat capacity), then the solid will melt, and finally the material is completely liquid (with a liquid heat capacity). This leads to the equation of state

$$T(\epsilon) = \begin{cases} \frac{\epsilon}{C_{v,\mathrm{s}}} & \epsilon < T_{\mathrm{m}} \cdot C_{v,\mathrm{s}} \\ T_m \quad T_m \cdot C_{v,\mathrm{s}} \leq & \epsilon \leq T_{\mathrm{m}} \cdot C_{v,\mathrm{s}} + L \\ \frac{\epsilon - L}{C_{v,\mathrm{l}}} & \epsilon > T_{\mathrm{m}} \cdot C_{v,\mathrm{s}} + L, \end{cases} \tag{7}$$

where $C_{v,\mathrm{s}}$ and $C_{v,\mathrm{l}}$ are the solid and liquid heat capacities, $T_{\mathrm{m}}$ is the melting temperature, and $L$ is the enthalpy of fusion. This equation of state is similar to the enthalpy method [11] commonly used in phase-change problems.

To investigate whether this equation of state, together with the energy-conserving DPD model presented in the previous section, will properly simulate the phase change of a material, the model will be tested against an analytical solution of a well-known problem [12]. Generally, these problems are fairly simple and consider a one-dimensional phase change by heat conduction only. This implies that only the last two terms of Eq. (3), describing the evolution of energy, will be employed. Physically this means that particles are on fixed positions during the simulation.

## 3. SIMULATIONS

In this section results of the simulation of phase-change DPD will be shown. First, the mapping of the thermal conductivity emerging from the energy-conserving DPD model is

shown, and a novel boundary condition method is explained. Finally, the simulation results of the phase-change DPD model are compared with the results calculated with the analytical solution.

### 3.1. *Mapping the Thermal Conductivity*

An important aspect of applying DPD to realistic science problems is the mapping of the DPD parameters on physical parameters. As explained before, one of the parameters in the energy-conserving DPD model is the thermal conductivity $\tilde{\kappa}$. In the article of Ripoll *et al.* [13] this parameter is mapped in the following way: a simulation is performed until a steady-state profile is reached between two thermal baths. Subsequently the heat flux is calculated for different thermal gradients. From a plot of the heat flux versus the imposed thermal gradient, the slope, representing the thermal diffusivity, is determined. Unfortunately, many simulations have to be performed to determine the thermal diffusivity. Furthermore, our aim for energy-conserving DPD is to perform time-dependent DPD simulations, which by definition a phase-change problem is. It is not demonstrated that this is possible in an accurate way, if the thermal diffusivity is determined from a steady-state solution.

In this paper, the thermal diffusivity is determined from (in principle) a single simulation. We choose the following system: suppose a solid body occupying the space from $x = 0$ to $x = \infty$ is initially at temperature $T_0$. At time $t = 0$, the temperature at $x = 0$ is raised to $T_1$ and kept at this temperature. Heat will penetrate the solid body by conduction only. The differential equation governing this one-dimensional problem is

$$\frac{\partial T}{\partial t} = a \frac{\partial^2 T}{\partial x^2} \tag{8}$$

with $a$ as the thermal diffusivity of the solid. The solution of this problem (see, for instance, [14]) is

$$\frac{T - T_0}{T_1 - T_0} = 1 - \frac{2}{\sqrt{\pi}} \int_0^{x/\sqrt{4at}} \exp(-\eta^2)\, d\eta = 1 - \operatorname{erf}\left(\frac{x}{\sqrt{4at}}\right) = \operatorname{erfc}\left(\frac{x}{\sqrt{4at}}\right). \tag{9}$$

The thermal diffusivity can now be found instantly from a single energy-conserving DPD simulation by fitting this formula onto a simulated temperature profile, at a certain time.

*3.1.1. Standard boundary condition.* The analytical solution given in the previous section is strictly valid only for an infinite system, but for short times it represents finite systems well. The simulations of Eq. (3) with the equation of state of a solid (Eq. (6)) are performed on a system with length $10 \times 5 \times 5$, containing 1250 particles. The boundary conditions are imposed, as suggested by Ripoll *et al.* [13], through an extra layer (size $r_c = 1.0$) of particles in which the particles are kept at a constant temperature. After the simulation of a certain time $t$ with a given thermal conductivity $\tilde{\kappa}$, the results are used to perform a nonlinear least-square fit (using the Levensberg–Marquardt method), to find the thermal diffusivity $a$ as used in Eq. (9).

In Fig. 1 results of these simulations are depicted for two simulation times. The temperatures are determined by averaging over bins that divide the $x$-axis. It is clear from this figure

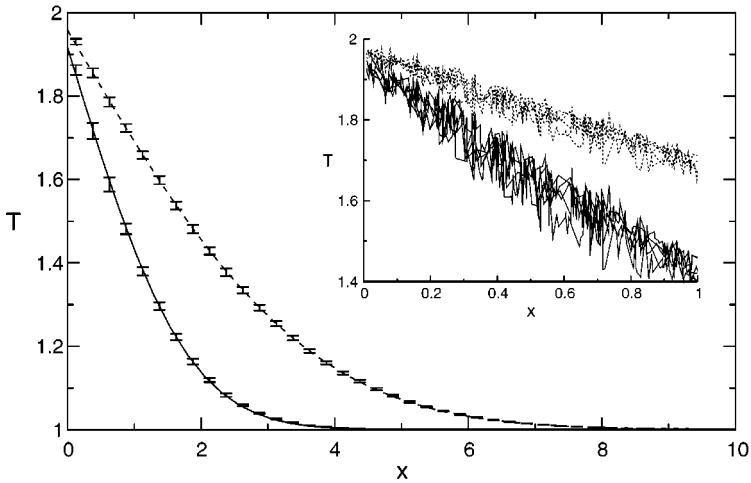


**FIG. 1.** Average temperature of the particles in the 40 bins dividing the $x$-axis. The error bars are determined by repeating the simulation five times. Two simulation times (solid line $t_1 = 10$ and dashed line $t_2 = 40$) are plotted. The close-up shows the nonaveraged temperature of every particle close to the wall.

that the boundary condition at $x = 0$ is not reproduced correctly. Instead of staying at the desired temperature ($T = 2.0$), it starts with a 10% difference (of the imposed temperature gradient), moving to the true value as time progresses, but never reaching it completely. This behaviour was never observed by Ripoll *et al.* since their work focused on low overlapping coefficients $s = r_c/\lambda$. The temperature slip can be explained as follows. Consider the system after it has reached steady state at the correct boundary value. In this situation the heat flowing to a particle equals that flowing from a particle. In the middle of the simulation box this condition is satisfied since the temperature profile is a straight line. Focusing on the particles close to the boundary, a straight temperature profile is now only possible at low overlapping coefficients. At higher overlapping coefficients (and thus many particles in the boundary), the temperature profile has a slope within the simulation box but is flat inside the boundary. Thus, a particle near the boundary loses a lot of energy to the particles toward the middle of the simulation box, while hardly gaining energy from the boundary. Therefore the steady-state temperature of the particles near the boundary is lower than intended.

*3.1.2. Consistent boundary condition.* It is clear that the implementation of boundary conditions, as used until now, does not impose the desired constant temperature correctly. The explanation of the incorrect implementation of the boundary condition given above immediately leads to the solution of the problem. Obviously, the particles near the boundary should still be subject to a heat flow from the boundary even when they have reached the boundary temperature. This is achieved by copying all the particles within a distance $r_c$ from the boundary into the extra layer. They are given the same $y, z$-position, and their $x$-position is mirrored with respect to the $x$-position of the boundary. The temperature of the particles is changed in such a way that the average temperature of the original and the mirrored particle is equal to the desired boundary temperature. In this case $T = 2$ at $x = 0$ and $T = 1$ at $x = L$.

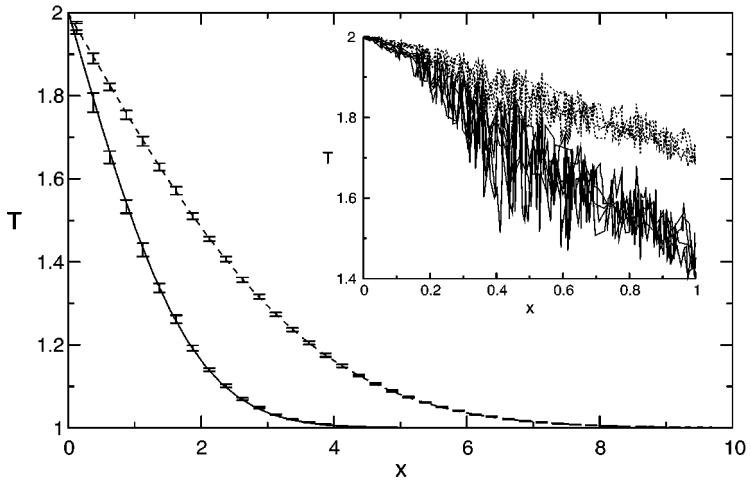


**FIG. 2.** Average temperature of the particles in the 40 bins that divide the $x$-axis using the consistent boundary condition. The error bars are determined by repeating the simulation five times. Two simulation times (solid line $t_1 = 10$ and dashed line $t_2 = 40$) are plotted. The close-up shows the nonaveraged temperature of every particle close to the wall.

In Fig. 2 simulation results are shown after the implementation of the new boundary condition. The resulting boundary temperature is reproduced correctly this time. The small price to pay lies in the stronger fluctuations at some distance from the boundary as compared to the original boundary condition. This is caused by the mirroring of the particles, leading to an increase of the density fluctuations near the boundary. These higher density fluctuations give rise to larger fluctuations in the temperature at some distance from the boundary. However, at the boundary the temperature fluctuations are smaller than with the previous method.

*3.1.3. Results from time-dependent fit.* The time-dependent heat transfer problem described by Eq. (9) can be correctly simulated with the consistent boundary condition. From these results it is possible to determine the thermal conductivity $a$. The following graph is constructed to prove the possibility of determining the thermal conductivity as described before. A simulation is performed on a system with length $40 \times 5 \times 5$, containing 10,000 particles. At a few time intervals the temperature profile is plotted. With the temperature profile of the first time interval, the thermal conductivity $a$ is determined. This value of $a$ is used to predict the temperature profile at the other two time intervals. As can be seen from Fig. 3, the agreement between the simulations and the predicted temperature profile is good. Notice that in this case only a single temperature profile has been used to determine the thermal conductivity. But to get some insight in the accuracy of this value, it can be determined from temperature profiles at different simulation times.

A kinetic-theory-based prediction (Ripoll *et al.* [13]) is given for the dependence of the thermal diffusivity on the overlapping coefficient and the thermal diffusivity $\tilde{\kappa}$:

$$a = \frac{s^2}{24}\tilde{\kappa}. \tag{10}$$

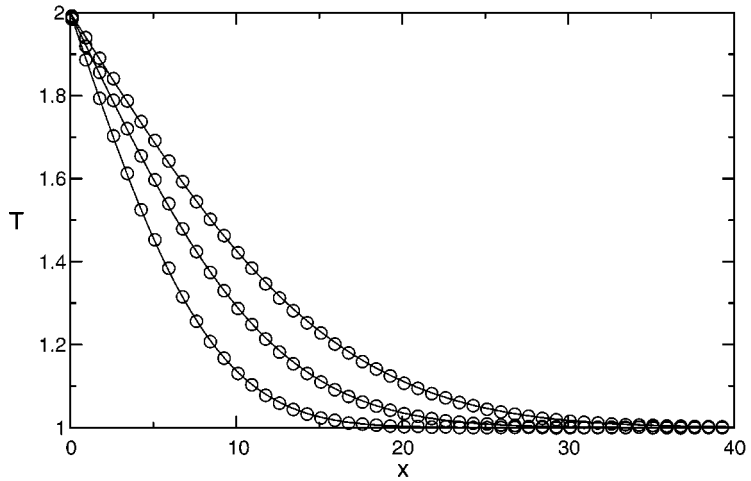


**FIG. 3.** Average temperature of the particles in the bins that divide the $x$-axis. The symbols represent the simulation results, and the lines give the prediction based on the fit performed on the first temperature profile. Three simulation times (125, 250, and 450) are plotted.

Using the thermal bath approach, Ripoll *et al.* found that the thermal diffusivity approximates the theoretical prediction for higher $s$-values, but never reaches it completely. Therefore, with the novel boundary condition several simulations have been performed at different overlapping coefficients. In Fig. 4 the results from these calculations have been plotted, as well as the theoretical prediction and the original data of Ripoll *et al.* [13].

It can be seen that the theoretical and simulation results agree for sufficiently high values of the overlapping coefficient.

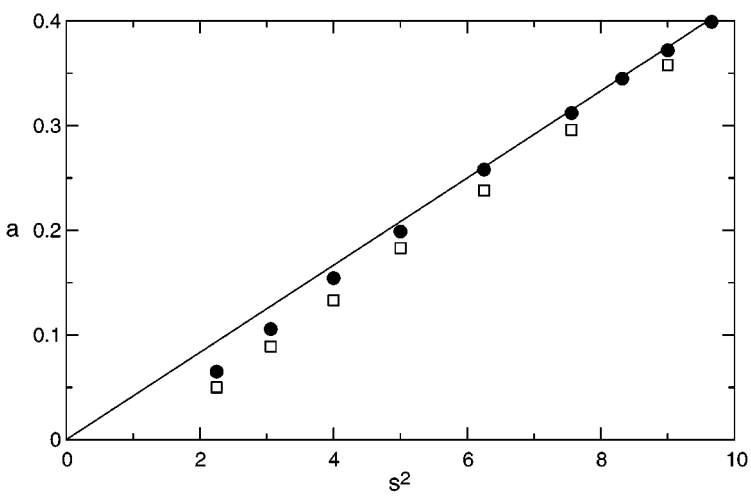


**FIG. 4.** Thermal diffusivity for different values of the overlapping coefficient with the consistent boundary conditions (closed symbols) and the original data from Ripoll *et al.* [13] (open symbols). The kinetic-theory-based prediction is also shown (solid line).

### 3.2. *Phase-Change DPD*

In this section the phase-change DPD scheme, as developed in Section 2.2, will be tested.

*3.2.1. Description of analytical model.* Freezing and melting have been described by Stefan [15] in the context of polar ice thickness prediction. Neumann [12] extended the mathematical description of the Stefan problem to the following test case. Suppose a solid body, occupying the space from $x = 0$ to $x = \infty$, is initially at temperature $T_0$, lower than the melting temperature $T_m$ of the substance. At time $t = 0$, the temperature at $x = 0$ is raised to $T_1$, above $T_m$, and kept at this temperature. A melting front $X$ with temperature $T_m$ will move into the solid. To describe mathematically the temperature evolution, two heat-conduction equations similar to Eq. (8) are required, one for the liquid region, occupying space between $x = 0$ and $x = X(t)$, and one in the solid region $x > X(t)$. Solving these equations requires an additional boundary condition,

$$k_s \frac{\partial T}{\partial x} = k_l \frac{\partial T}{\partial x} + L\rho \frac{dX}{dt} \tag{11}$$

with $k_s$ and $k_l$ as the thermal conductivity of the solid and liquid, respectively (assumed to be equal in this case), $\rho$ as the density, and $L$ as the enthalpy of fusion. This boundary condition states that the melting rate is equal to the difference of heat flow towards and from the melting front. The solution of this problem is expressed in terms of the moving interface position,

$$X(t) = 2\xi\sqrt{a_l t}, \tag{12}$$

the temperature in the liquid phase,

$$\frac{T - T_1}{T_1 - T_m} = 1 - \frac{\operatorname{erf}(x/\sqrt{4a_l t})}{\operatorname{erf}(\xi)}, \tag{13}$$

and the temperature in the solid phase,

$$\frac{T - T_0}{T_m - T_0} = 1 - \frac{\operatorname{erfc}(x/\sqrt{4a_s t})}{\operatorname{erfc}(\xi\sqrt{(a_l/a_s)})}. \tag{14}$$

The $\xi$ in these equations is the root of

$$\frac{C_{v,l}(T_1 - T_m)}{\exp(\xi^2)\operatorname{erf}(\xi)} - \frac{C_{v,s}\sqrt{a_s}}{\sqrt{a_l}\exp(\xi^2(a_l/a_s))\operatorname{erfc}(\xi\sqrt{a_l/a_s})} = L\xi\sqrt{\pi}. \tag{15}$$

In the next section, the results from phase-change DPD simulations will be compared with the results from these analytical solutions.

*3.2.2. Results.* For short times, the analytical solutions given in the previous section can be compared to simulations performed in a finite system. The simulations of Eq. (3) with the equation of state incorporating phase change (Eq. (7)) are performed on a system with length $40 \times 5 \times 5$, containing 10,000 particles. The enthalpy of fusion $L = 5$, $C_v = 5$, and $T_m = 1.5$.

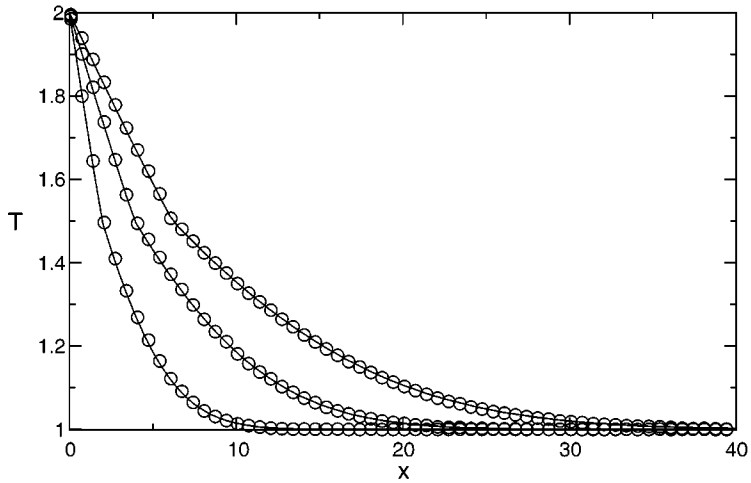


**FIG. 5.** Average temperature of the particles in the bins that divide the $x$-axis. The symbols represent the simulations, and the solid lines are the analytical results. Three simulation times (50, 200, and 500) are plotted.

In Fig. 5 results of these simulations are depicted for three simulation times. One observes good agreement between the simulations and the analytical results. At the melting temperature ($T_m = 1.5$) a discontinuity in the temperature profile is observed. This is caused by the removal of heat that is used for melting the material, in accordance with Eq. (11). Notice that these simulations did not require any fitting. The thermal conductivity has been determined from the one-phase simulations. The position of the melting front is determined by monitoring the $x$-position of the melting temperature in time. In Fig. 6 this is shown together with the analytical solution. Again the agreement is very good.

From these two graphs it can be concluded that the described extension to the original energy-conserving DPD scheme allows us to successfully perform phase-change calculations.

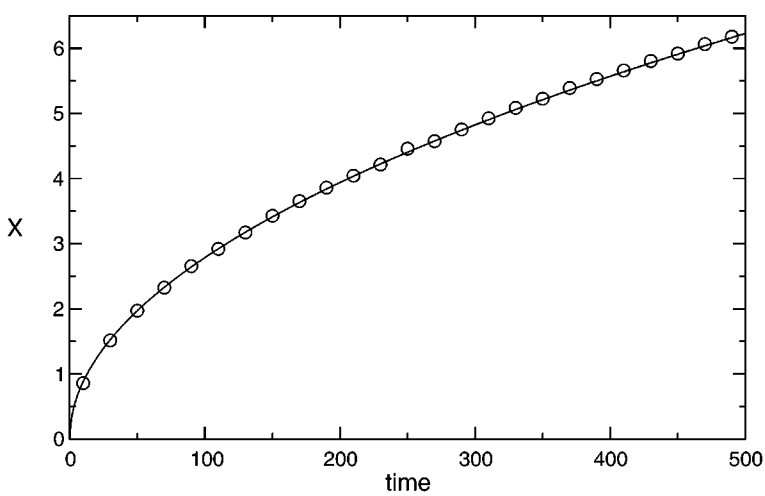


**FIG. 6.** Evolution of the melting front in time. The symbols represent the simulations while the solid line represents the analytical solution.

## 4. CONCLUDING REMARKS

We investigated the possibility of simulating phase change with DPD. To achieve this, an extension to the original energy-conserving DPD has been proposed. In order to properly account for the different phases involved, i.e., solid, liquid, and melting states, the equation of state has been divided into three parts. Concerning our objective to perform accurate time-dependent calculations, it was found that the commonly used implementation of a constant temperature boundary condition can yield incorrect results at high overlapping coefficients. In this paper a new consistent boundary condition has been introduced and applied successfully for all overlapping coefficients. In conventional DPD simulations the problem of wall-slip was first noticed by Revenga *et al.* [16]. Our new approach to implementing boundary conditions can also solve this problem [17].

## ACKNOWLEDGMENT

Financial support provided by DSM Research is gratefully acknowledged.

## REFERENCES

1. P. J. Hoogerbrugge and J. M. V. A. Koelman, Simulating microscopic hydrodynamics phenomena with dissipative particle dynamics, *Europhys. Lett.* **19**(3), 155 (1992).
2. J. M. V. A. Koelman and P. J. Hoogerbrugge, Dynamic simulation of hard-sphere suspensions under steady shear, *Europhys. Lett.* **21**(3), 363 (1993).
3. A. G. Schlijper, P. J. Hoogerbrugge, and C. W. Manke, Computer simulation of dilute polymer solutions with the dissipative particle dynamics method, *J. Rheol.* **39**(3), 567 (1995).
4. K. E. Novik and P. V. Coveney, Using dissipative particle dynamics to model binary immiscible fluids, *Int. J. Mod. Phys. C* **8**(4), 909 (1997).
5. S. M. Willemsen, T. J. H. Vlugt, H. C. J. Hoefsloot, and B. Smit, Combining dissipative particle dynamics and Monte Carlo techniques, *J. Comp. Phys.* **147**, 507 (1998).
6. P. Español and P. Warren, Statistical mechanics of dissipative particle dynamics, *Europhys. Lett.* **30**(4), 191 (1995).
7. P. Español, Hydrodynamics from dissipative particle dynamics, *Phys. Rev. E* **52**(2), 1734 (1995).
8. C. A. Marsh, G. Backx, and M. H. Ernst, Static and dynamic properties of dissipative particle dynamics, *Phys. Rev. E* **56**(2), 1676 (1997).
9. J. B. Avalos and A. D. Mackie, Dissipative particle dynamics with energy conservation, *Europhys. Lett.* **40**(2), 141 (1997).
10. P. Español, Dissipative particle dynamics with energy conservation, *Europhys. Lett.* **40**(6), 631 (1997).
11. V. R. Voller and C. Prakash, A fixed grid numerical modelling methodology for convection–diffusion mushy region phase-change problems, *Int. J. Heat Mass Transfer* **30**(8), 1709 (1987).
12. F. Neumann, *Die Partiellen Differentialgleichungen der Mathematischen Physic*, Vol. 2 (Reimann & Weber, 1912).
13. M. Ripoll, P. Español, and M. H. Ernst, Dissipative particle dynamics with energy conservation: Heat conduction, *Int. J. Mod. Phys. C* **9**(8), 1329 (1998).
14. R. B. Bird, W. E. Stewart, and E. N. Lightfoot, *Transport Phenomena* (Wiley, New York, 1960).
15. J. Stefan, Uber die theorie der eisbildung, insbesondere uber die eisbildung im polarmeer, *Ann. Chem. Phys.* **42**, 269 (1891).
16. M. Revenga, I. Zúñiga, P. Español, and I. Pagonabarraga, Boundary models in DPD, *Int. J. Mod. Phys. C* **9**(8), 1319 (1998).
17. S. M. Willemsen, H. C. J. Hoefsloot, and P. D. Iedema, No-slip boundary condition in dissipative particle dynamics, submitted.